

## Article

# Characterization and Prediction of Water Stress Using Time Series and Artificial Intelligence Models

Amuktamalyada Gorlapalli <sup>1,†</sup>, Supriya Kallakuri <sup>1,\*,†</sup>, Pagadala Damodaram Sreekanth <sup>2</sup>, Rahul Patil <sup>3</sup>,  
Nirmala Bandumula <sup>4</sup>, Gabrijel Ondrasek <sup>5</sup>, Meena Admala <sup>1</sup>, Channappa Gireesh <sup>4</sup>,  
Madhyavenkatapura Siddaiah Anantha <sup>4</sup>, Brajendra Parmar <sup>4</sup>, Brahamdeo Kumar Yadav <sup>6</sup>,  
Raman Meenakshi Sundaram <sup>4</sup> and Santosha Rathod <sup>4,\*,†</sup>

- <sup>1</sup> College of Agriculture, Professor Jayashankar Telangana State Agricultural University, Hyderabad 500030, India; amuktamalyadasweetty@gmail.com (A.G.); meenaadmala22@gmail.com (M.A.)  
<sup>2</sup> ICAR—National Academy of Agricultural Research Management, Hyderabad 500030, India; sreekanth@naarm.org.in  
<sup>3</sup> College of Agricultural Engineering, University of Agricultural Sciences, Raichur 584104, India; rahul1235110@gmail.com  
<sup>4</sup> ICAR—Indian Institute of Rice Research, Hyderabad 500030, India; bnirmaladrr@gmail.com (N.B.); giri09@gmail.com (C.G.); anugenes@gmail.com (M.S.A.); birju1973@gmail.com (B.P.); rms\_28@rediffmail.com (R.M.S.)  
<sup>5</sup> Faculty of Agriculture, University of Zagreb, 10000 Zagreb, Croatia; gondrasek@agr.hr  
<sup>6</sup> Krishi Vigyan Kendra, Balumath, Latehar 829202, India; bd2511@gmail.com  
\* Correspondence: supriyakallakuri@gmail.com (S.K.); santosha.rathod@icar.gov.in (S.R.)  
† These authors contributed equally to this work.



**Citation:** Gorlapalli, A.; Kallakuri, S.; Sreekanth, P.D.; Patil, R.; Bandumula, N.; Ondrasek, G.; Admala, M.; Gireesh, C.; Anantha, M.S.; Parmar, B.; et al. Characterization and Prediction of Water Stress Using Time Series and Artificial Intelligence Models. *Sustainability* **2022**, *14*, 6690. <https://doi.org/10.3390/su14116690>

Academic Editor: Andrzej Walega

Received: 3 April 2022

Accepted: 25 May 2022

Published: 30 May 2022

**Publisher's Note:** MDPI stays neutral with regard to jurisdictional claims in published maps and institutional affiliations.



**Copyright:** © 2022 by the authors. Licensee MDPI, Basel, Switzerland. This article is an open access article distributed under the terms and conditions of the Creative Commons Attribution (CC BY) license (<https://creativecommons.org/licenses/by/4.0/>).

**Abstract:** In agroecosystems, drought is a critical climatic phenomenon that affects evapotranspiration and induces water stress in plants. The objective in this study was to characterize and forecast water stress in the Hyderabad region of India using artificial intelligence models. The monthly precipitation data for the period 1982–2021 was characterized by the standardized precipitation index (SPI) and modeled using the classical autoregressive integrated moving average (ARIMA) model and artificial intelligence (AI), i.e., artificial neural network (ANN) and support vector regression (SVR) model. The results show that on the short-term SPI3 time scale the studied region experienced extreme water deficit in 1983, 1992, 1993, 2007, 2015, and 2018, while on the mid-term SPI6 time scale, 1983, 1991, 2011, and 2016 were extremely dry. In addition, the prediction of drought at both SPI3 and SPI6 time scales by AI models outperformed the classical ARIMA models in both, training and validation data sets. Among applied models, the SVR model performed better than other models in modeling and predicting drought (confirmed by root mean square error—RMSE), while the Diebold–Mariano test confirmed that SVR output was significantly superior. A reduction in the prediction error of SVR by 48% and 32% (vs. ARIMA), and by 21% and 26% (vs. ANN) was observed in the test data sets for both SPI3 and SPI6 time scales. These results may be due to the ability of the SVR model to account for the nonlinear and complex patterns in the input data sets against the classical linear ARIMA model. These results may contribute to more sustainable and efficient management of water resources/stress in cropping systems.

**Keywords:** drought; water stress; standardized precipitation index; SPI3; SPI6; artificial intelligence; auto-regressive integrated moving average; artificial neural network; support vector regression

## 1. Introduction

Meteorological and hydrological droughts commonly cause agricultural drought, i.e., water stress in agroecosystems. The three longest droughts globally occurred between July 1928 and May 1942 (Dust Bowl drought of the 1930s), July 1949 and September 1957 (1950s drought), and between June 1998 and December 2014 (early 21st-century drought). However, the frequency of droughts has increased in recent decades, reducing

the productivity of the agri-food sector [1–3]. For example, in 2017 at least 3 percent of the world's land area was affected by extreme drought [4]. Drought is a complex natural hazard that affects global food security through water stress, making the agri-food sector one of the most affected by drought. Namely, water stress negatively affects many physiological functions of plants, including photosynthesis, transpiration, and nutrient uptake, and reduces vegetative growth and crop yield. Water stress is projected to worsen under global climate change and thus further threaten global food security [5–7]. Climate change is affecting the production of most agricultural commodities and it is projected to decline further [8].

Drought detection, characterization, and prediction via different approaches are critical for decision support systems and more successful drought, i.e., water management, and thus food security. Moreover, drought modeling and prediction can be a very useful tool for more sustainable water planning to avoid future uncertainties that may arise from water scarcity and stress [9], not only in agroecosystems but also in other sectors.

As a result, much attention has been dedicated to drought characterization and modeling, and continuous progress has been recorded in this field. However, a major research challenge still remains in the development of an appropriate approach to predicting the onset and termination of droughts, given the critical stage in mitigating the effects of drought is the inability to accurately predict drought conditions for the upcoming short-/medium-term period [9]. In addition, despite significant improvements in drought modeling in recent decades, not many studies have used advanced approaches, such as artificial intelligence (AI) modeling, to characterize and predict droughts. For example, many studies have used the standardized precipitation index (SPI) model developed by [10] to characterize drought. The author of [11] modeled climatological precipitation using the gamma distribution, ref. [12] studied hydrological drought using the SPI for medium and long time periods, while ref. [13] used the SPI to calculate long-term spatial and temporal trends in drought. Precipitation patterns were analyzed by [14] who studied drought severity using SPI, while ref. [15] characterized drought in Italy using SPI at different time scales. Furthermore, ref. [16] used SPI to study meteorological droughts for different climate models at different time scales. SPI for drought characterization using multi-satellite precipitation data from the Tropical Precipitation Measurement Mission were computed by [17]. SPI was developed by [18] for characterizing short and intermediate droughts, while ref. [19] characterized drought in the Lower Mekong Basin in Southeast Asia using SPI at different time scales. Drought conditions for maize in different growing seasons using SPI values in the Adana, Mersin, and Osmaniye regions of Çukurova were determined by [20], whereas ref. [21] applied SPI to calculate drought and heatwaves in China.

Box–Jenkins autoregressive integrated moving average (ARIMA) is the most commonly used time series model for predicting linear time series data [22]. There are many cases where ARIMA is used for modeling and forecasting drought and other agricultural phenomena [23–25]. However, the classical time series ARIMA model is not able to model the nonlinear, heterogeneous, and complex patterns present in the time series and does not provide reliable forecasts. Many nonparametric machine learning models have been developed and are available in the literature to solve the problem of modeling nonlinear components in time series data. However, the only approach to model and predict such time series is still the use of AI techniques [26–29]. Artificial neural networks (ANN) and support vector regression (SVR) is the most commonly used techniques for modeling and prediction of drought and other agricultural variables [23,30–34].

The Hyderabad region in the Indian state of Telangana is characterized by intensive agroecosystems affected by frequent drought and water stress [35]. According to recent reports, 7/10 districts were affected by drought (Association for India's development, 2016 survey report), threatening the water supply for food production and other industrial and municipal sectors. Therefore, the development of drought characterization and its prediction would greatly improve drought management at the multi-sectoral scale. For the selected Hyderabad region, this is the first attempt to model and predict drought, i.e.,

water stress, using AI techniques such as ANN and SVR. Moreover, this work was the first attempt to significantly compare the modeling performance of the studied techniques using the test of Diebold and Mariano [36]. The methodological framework begins with the characterization of drought by SPI. The AI-based ANN and SVR models presented here were developed to model and predict drought, not only in the Hyderabad region, but also in similar water-scarce and drought-affected agroecosystems. Thus, the results could serve as a valuable tool and extension in drought, i.e., water management, and food security.

## 2. Materials and Methods

### 2.1. Description of the Data and Study Area

The study pertains to Hyderabad, the capital city of Telangana state of India. Telangana has an area of 112,077 sq. km and has a population of 35,003,674. The state receives an average annual rainfall of about 1000 mm. The Hyderabad (17.3850° N, 78.4867° E) region of the Hyderabad region of the Telangana state is selected as the study area, as the average rainfall received by the region is usually less than the state average. The annual rainfall of the Hyderabad region was observed to be around 750 mm, the region receives most of its rainfall from the southwest monsoon. The monthly rainfall data (millimeter (mm)) in Hyderabad from January 1988 to May 2021, was obtained from the Directorate of Economics and Statistics, Government of Telangana. Further, the rainfall data is used to calculate the SPI for three and six-month time scales.

### 2.2. Standardized Precipitation Index (SPI)

The rainfall data were used to calculate the SPI indices for time scales of 3 (SPI3) and 6 (SPI6) months. The SPI was calculated based on the probability of precipitation for a specific time scale. The gamma distribution is defined by its frequency or probability density function.

$$f(x, \alpha, \beta) = \frac{1}{\beta^\alpha \Gamma(\alpha)} x^{\alpha-1} e^{-\left(\frac{x}{\beta}\right)} \quad (1)$$

where,  $\alpha$  and  $\beta$  are the shape and scale parameters respectively;  $x$  is the rainfall amount (millimeter), and  $\Gamma(\alpha)$  is the gamma function,  $\alpha > 0$ ,

$$\Gamma(\alpha) = \int_0^\infty x^{\alpha-1} e^{-x} \quad (2)$$

where,  $\Gamma(\alpha)$  is the gamma function.

Computation of the SPI was mainly involved in fitting a gamma probability density function to a given frequency distribution of precipitation. The maximum likelihood solutions used for optimal estimation of  $\alpha$  and  $\beta$  are given as follows [9]:

$$\alpha = \frac{1}{4A} \left( 1 + \sqrt{1 + \frac{4A}{3}} \right) \cdot \alpha > 0, \quad (3)$$

$$\beta = \frac{\bar{x}}{\alpha}, \quad \beta > 0 \quad (4)$$

$$A = \ln(\bar{x}) - \frac{\sum_{i=1}^n \ln(x)}{n}, \quad (5)$$

where,  $n$  = number of precipitation observations.

Integrating the probability density function with respect to  $x$  and attaching  $\alpha$  and  $\beta$  parameters yields the cumulative probability distribution function  $F(x)$ :

$$F(x, \alpha, \beta) = \int_0^x f(x, \alpha, \beta) = \frac{1}{\beta^\alpha \Gamma(\alpha)} \int_0^x x^{\alpha-1} e^{-\left(\frac{x}{\beta}\right)} dx \quad (6)$$

Equation (6) can be expressed as follows:

$$F(x, \alpha, \beta) = \frac{1}{\Gamma(\alpha)} \int_0^x t^{\alpha-1} e^{-(t)} dx \quad (7)$$

where,  $t = x/\beta$ .

Since the gamma function is undefined for  $x = 0$  and the rainfall time series data may contain zero rainfalls, the cumulative probability of zero and non-zero rainfalls,  $H(x)$  can be calculated as:

$$H(x) = q + (1 - q)F(x, \alpha, \beta) \quad (8)$$

where,  $q$  is the probability of zero rainfall. If  $m$  is the number of zeros present in a rainfall time series, then  $q$  is estimated by  $m/n$ . The cumulative probability was then transformed into a standard normal random variable  $Z$ , then its mean is 0 and variance is 1, which is the value of the SPI.

Ref. [37] derived the following equations to transform the cumulative probability distribution into a standardized normal distribution to calculate the SPI as follows:

$$\text{SPI} = - \left( K - \frac{c_0 + c_1 K + c_2 K^2}{1 + d_1 + d_2 k^2 + d_3 K^3} \right) \text{ when } K = \sqrt{\ln \left( \frac{1}{(H(x))^2} \right)} \quad (9)$$

for  $0 < H(x) \leq 0.5$

$$\text{SPI} = + \left( K - \frac{c_0 + c_1 K + c_2 K^2}{1 + d_1 + d_2 k^2 + d_3 K^3} \right) \text{ when } K = \sqrt{\ln \left( \frac{1}{1 - (H(x))^2} \right)} \quad (10)$$

for  $0.5 < H(x) \leq 1$

where,  $C_0 = 2.515517$ ,  $C_1 = 0.802853$ ,  $C_2 = 0.010328$ ,  $d_1 = 1.432788$ ,  $d_2 = 0.189269$ , and  $d_3 = 0.001308$ . The SPI for time scales 3 (SPI3) and 6 (SPI6) represent short-term and mid-term meteorological droughts, respectively [37]. The SPI is categorized in to different groups as mention in Table 1 below:

**Table 1.** Category of Standardized precipitation index.

SPI Range	Category
+2 to more	Extremely wet
1.5 to 1.99	Very wet
1.0 to 1.49	Moderately wet
−0.99 to 0.99	Near normal
−1.0 to −1.49	Moderately dry
−1.5 to −1.99	Severely dry
−2 to less	Extremely dry

SPI: standardized precipitation index.

After the development of SPI3 and SPI6, the indexes from January 1982 to May 2020 were considered as the training dataset (data for model building), while the indexes from June 2020 to May 2021 were considered as the testing dataset (data for model validation) in this study.

### 2.3. ARIMA Model

The ARIMA model was characterized by three terms:  $p$ ,  $d$ , and  $q$ , where, ' $p$ ' is the order of the 'auto regressive' (AR) term, referring to the number of lags of  $Y_t$  time series to be used as predictors. ' $q$ ' is the order of the 'moving average' (MA) term, assuming the number of lagged forecast errors that should go into the ARIMA model. ' $d$ ' is the number

of differences required to make the time series stationary; the most common approach of differencing is, subtract the previous value from the current value.

$$\varnothing(B)(1 - B)^d Y_t = \theta(B)e_t \quad (11)$$

$$Y_t = \varnothing_1 Y_{t-1} + \varnothing_2 Y_{t-2} + \dots + \varnothing_p Y_{t-p} + \varepsilon_t - \theta_1 e_{t-1} - \theta_2 e_{t-2} - \dots - \theta_q e_{t-q} \quad (12)$$

where,  $Y_t$  is the time series,  $\varnothing_i$  and  $\theta_j$  are model parameters for AR and MA terms, respectively,  $e_t$  is the random error,  $p$  is a number of autoregressive terms,  $q$  is number of lagged forecast errors, and  $B$  is the backshift operator such that  $BY_t = Y_{t-1}$ . The ARIMA model building consists of four stages, viz. identification, estimation, diagnostic checking, and forecasting [22].

#### 2.4. Artificial Neural Network (ANN)

The ANN is one of the most widely used artificial intelligence techniques in the last two decades, for both classification and regression tasks. As time-series falls under regression problem, the lagged autoregressive observations were used as input to the network with an implicit functional representation of time. The mathematical expression for the output  $Y_t$  of a single-layer or multi-layer feed-forward autoregressive network is expressed as follows:

$$Y_t = \alpha_0 + \sum_{j=1}^q \alpha_j g \left( \beta_{0j} + \sum_{i=1}^p \beta_{ij} Y_{t-i} \right) + e_t \quad (13)$$

where,  $\alpha_j (j = 0, 1, 2, \dots, q)$  and  $\beta_{ij} (i = 0, 1, 2, \dots, p, j = 0, 1, 2, \dots, q)$  are the model parameters,  $p$  is the number of input nodes,  $q$  is the number of hidden nodes,  $g$  is the activation function, and  $e_t$  is the random error [38]. The logistic function is the most commonly used activation function in time series modeling.

$$g = \frac{1}{1 + \exp(-x)} \quad (14)$$

The ANN model building was generally divided into the model building part (training data set) and validation part (testing set). In model building, the algorithm minimizes the error function between actual and predicted values. The error function was expressed as follows:

$$E = \frac{1}{N} \sum_{t=1}^N (e_t)^2 = \frac{1}{N} \sum_{t=1}^N \{X_t - (w_0 + (\sum_{j=1}^Q w_j g(w_{0j} + \sum_{i=1}^P w_{ij} X_{t-i})))\}^2 \quad (15)$$

where,  $N$  is the total number of error terms and  $w_{ij}$  are the weight parameters of the neural network which are changed by a number of changes in  $\Delta w_{ij} = -\eta \frac{\partial E}{\partial w_{ij}}$  where  $\eta$  is the learning rate which is a user-defined hyper-parameter [39,40]. The schematic representation of the autoregressive feed-forward neural network is depicted in Figure 1.

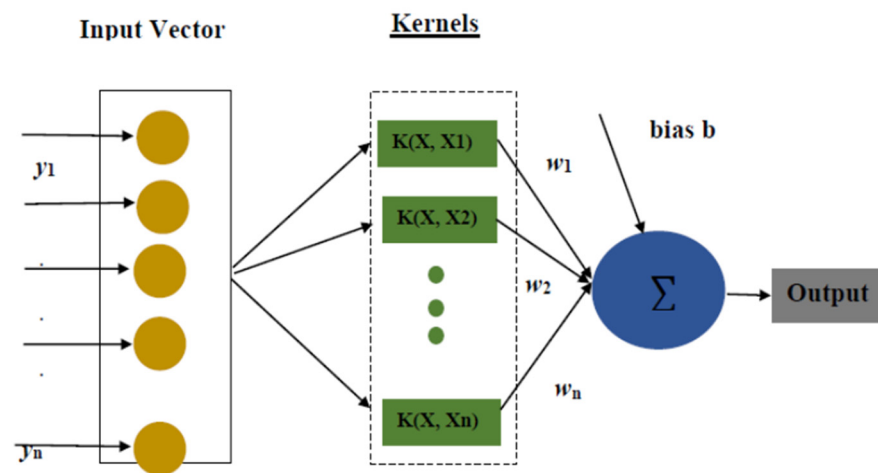


**Figure 1.** Feed-forward neural network architecture.

### 2.5. Support Vector Regression (SVR)

The support vector regression (SVR) is a supervised machine learning technique originally developed for binary classification and later extended to nonlinear regression estimation problems by introducing an  $\varepsilon$ -insensitive loss function [41]. The basic principle involved in NLSVR (nonlinear SVR) is to transform the original input time series into a high dimensional feature space and then build the regression model in a new feature space.

Consider a vector of data set  $Z = \{x_i, y_i\}_{i=1}^N$  where  $x_i \in R^n$  is an input vector,  $y_i$  is the scalar output, and  $N$  is the size of data set. The general equation SVR can be written as follows [41]:

$$f(x) = W^T \phi(x) + b \quad (16)$$

where,  $\phi(x)$  is function of  $x$ ,  $W$  is weight vector,  $b$  is bias term, and superscript  $T$  denotes the transpose. The coefficients  $W$  and  $b$  were estimated by minimizing the following regularized risk function:

$$R(\theta) = \frac{1}{2} \|w\|^2 + C \left[ \frac{1}{N} \sum_{i=1}^N L_\varepsilon(y_i, f(x_i)) \right] \quad (17)$$

The first term  $\frac{1}{2} \|w\|^2$  is called 'regularized term', which measures the flatness of the function. Minimization of the regularized terms will make a function as flat as possible. The second term  $\frac{1}{N} \sum_{i=1}^N L_\varepsilon(y_i, f(x_i))$  is called as 'empirical error' or loss function  $L_\varepsilon$  which was estimated by Vapnik  $\varepsilon$ -insensitive loss function as follows:

$$L_\varepsilon(y_i, f(x_i)) = f(x) = \begin{cases} |y_i, f(x_i) - \varepsilon|; & |y_i - f(x_i)| \geq \varepsilon, \\ 0; & |y_i - f(x_i)| < \varepsilon, \end{cases} \quad (18)$$

where,  $y_i$  is the actual value,  $f(x_i)$  is the estimated value, and  $\varepsilon$  is the margin of tolerance where no penalty is given to errors.

The kernel function in SVR plays a critical role in mapping the input to output, where the information is processed using a suitable kernel function. The most commonly used kernel functions radial basis function (RBF)  $K$  is given as follows:

$$K(Y_1, Y_2) = \exp\left(-\frac{(\|x_1 - x_2\|)^2}{2\sigma^2}\right) \quad (19)$$

where,  $\sigma^2$  is the variance, and  $\|x_1 - x_2\|$  is the Euclidean distance between two sample points  $x_1$  and  $x_2$ . The performance of SVR depends upon the optimization of two hyper-parameters; regularization parameter  $C$  also called the cost function, which balances the

complexity and approximation accuracy of the model and kernel bandwidth parameter  $\gamma = \frac{1}{2\sigma^2}$ , which represents the variance of the kernel function.

Finally, a general flow chart of the methodology followed in this study is delineated in Figure 2. The flow chart depicts the development of drought indices SPI3 and SPI6 using rainfall data, modeling, and forecasting of drought using different models and performance of models in both training and testing data sets in terms of RMSE and Diebold–Mariano (DM) test.

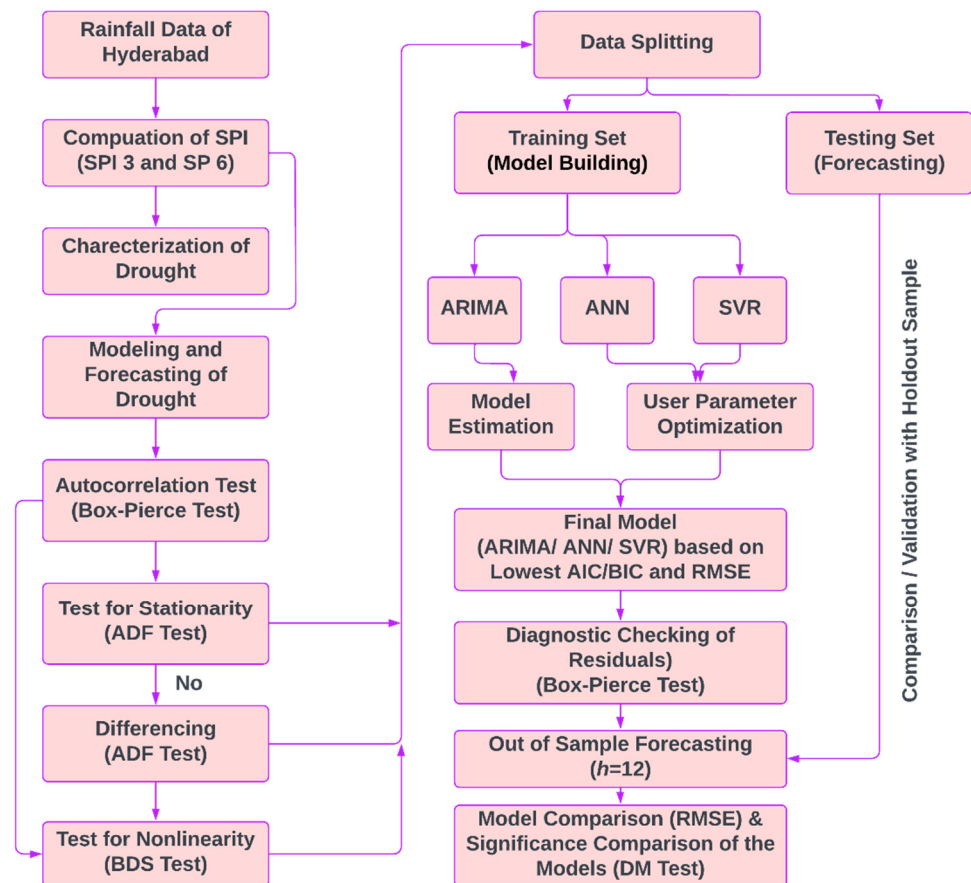
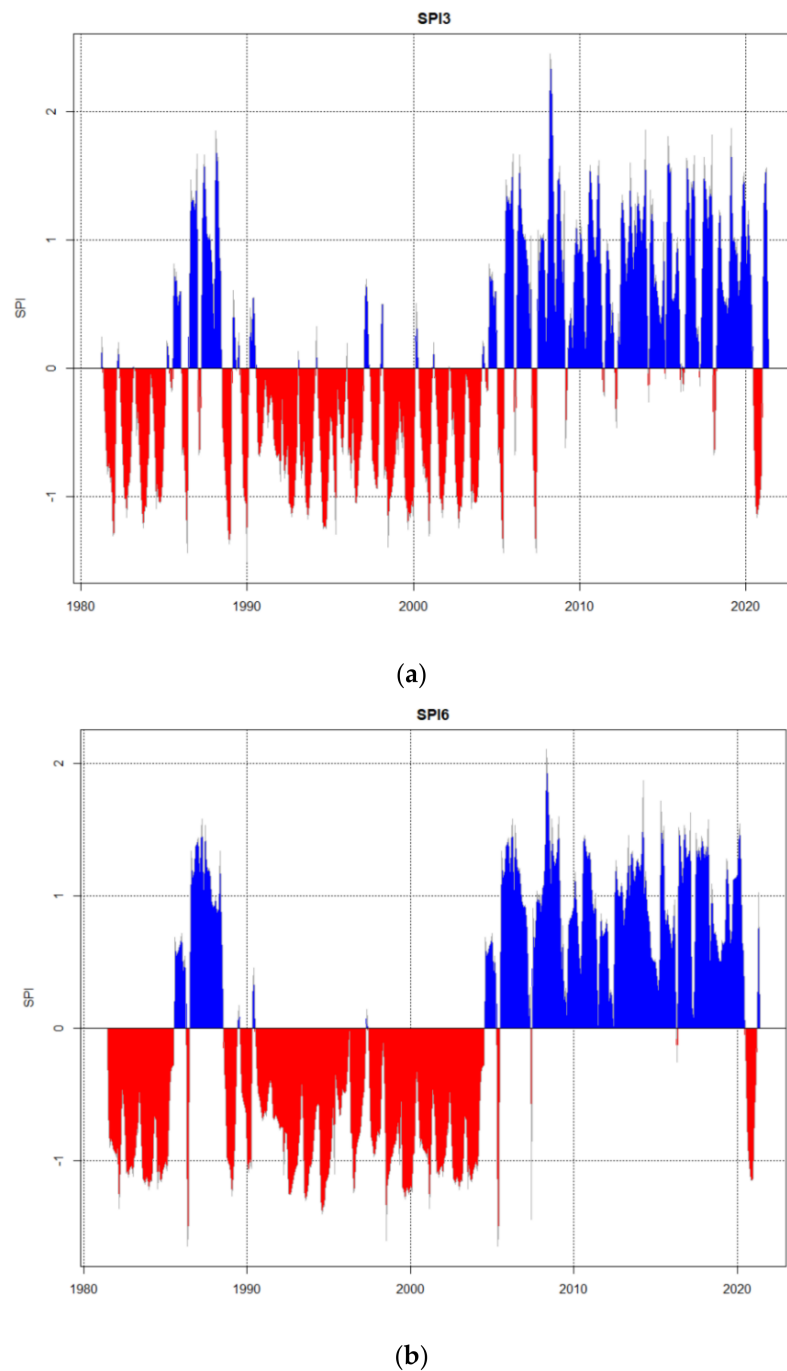


Figure 2. Schematic representation of proposed methodology.

### 3. Results

#### 3.1. Calculated SPI

The calculated water stress indexes for SPI3 and SPI6 timescales (Table S1) are plotted in Figure 3a,b, respectively. The drought events were developed from 1982 to 2021 for both SPI3 and SPI6 timescales (Tables 2 and 3). For instance, ten months in 1983 (−2.24 SPI3\_Feb, −2.25 SPI3\_Mar, −3.15 SPI3\_Apr, −2.13 SPI3\_May), 1992 (−2.06 SPI3\_Mar), 1993 (−2.04 SPI3\_Feb), 2007 (−2.08 SPI3\_Mar), 2015 (−2.25 SPI3\_Jul), and 2018 (−2.08 SPI3\_Jan, −2.49 SPI3\_Feb) experienced extreme water stress on SPI3 time scale (Table 2, Figure 3a). In addition, on the same scale during 1982, 1983, 1984, 1985, 1988, 1989, 1990, 1992, 1993, 1994, 1997, 1998, 1999, 2002, 2003, 2004, 2010, 2018, and 2019 were recorded as moderately dry, while in 1983, 1984, 1990, 1991, 1998, 2003, 2010, 2018, and 2019, severely dry conditions were observed (Table 2).



**Figure 3.** (a) SPI3 water stress index; (b) SPI6 water stress index.

On the other hand, SPI6 indicates medium-term drought conditions, and on this time scale there were four months with extreme water stress in 1983 ( $-2.66$  SPI6\_May), 1991 ( $-2.42$  SPI6\_May), 2011 ( $-2.20$  SPI6\_June), and 2016 ( $-2.38$  SPI6\_Mar), moderately dry conditions were confirmed in 1983, 1985, 1989, 1990, 1996, 2000, 2002, and 2003, while severely dry conditions were recorded in 1986, 2002, 2003, 2007, 2011, 2018, and 2019 (Table 3, Figure 3b).

**Table 2.** Calculated drought months by short-term SPI3.

Year	Jan	Feb	Mar	Apr	May	Jun	Jul	Aug	Sep	Oct	Nov	Dec
1982										−1.21		
1983	−1.56	−2.04	−2.25	−3.15	−2.13				−1.30	−1.48		
1984						−1.56	−1.23	−1.89				
1985												−1.15
1988												−1.30
1989	−1.19	−1.43		−1.22							−1.08	−1.34
1990	−1.34	−1.64	−1.78	−1.17								
1991			−1.51									
1992			−2.06			−1.11	−1.49					
1993			−2.04			−1.12	−1.71					
1994										−1.21		
1997								−1.30	−1.48			
1998					−1.60	−1.00	−1.92					
1999											−1.14	
2002										−1.26		
2003			−1.37			−1.48	−1.67					
2004									−1.15		−1.13	
2007			−2.08									
2010				−1.32	−1.67							
2015							−2.25					
2018	−2.08	−2.49							−1.27	−1.97	−1.11	−1.80
2019	−1.12				−1.82	−1.66						

Jan: January, Feb: February, Mar: March, Apr: April, Jun: June, Jul: July, Aug: August, Sep: September, Nov: November, Dec: December.

**Table 3.** Calculated drought months by mid-term SPI6.

Year	Jan	Feb	Mar	Apr	May	Jun	Jul	Aug	Sep	Oct	Nov	Dec
1983	−1.18	−1.08			−2.66							
1985						−1.37	−1.33	−1.36				
1986										−1.86	−1.53	
1989	−1.27	−1.35	−1.19									
1990	−1.11	−1.18										
1991					−2.42							
1996							−1.37	−1.28	−1.07			
2000									−1.08		−1.02	−1.04
2002								−1.21	−1.86	−1.56		−1.98
2003	−1.72	−1.24										
2007						−1.53						
2011		−2.20	−1.85									
2016			−2.66									
2018											−1.95	−1.62
2019	−1.66											

Jan: January, Feb: February, Mar: March, Apr: April, Jun: June, Jul: July, Aug: August, Sep: September, Nov: November, Dec: December.

### 3.2. ARIMA Model

The time series plots of SPI at 3 and 6 timescales are depicted in Figure 4a,b. The time series modeling ‘Box–Pierce test’ was performed to check the autocorrelation of the series using the following formula [22]:

$$Q = n(n + 2) \sum_{k=1}^h \frac{\hat{\rho}_k^2}{n - k} \tag{20}$$

where  $n$  is the sample size,  $\hat{\rho}_k$  is the sample autocorrelation at lag  $k$ , and  $h$  is the number of lags being tested; and  $Q$  follows  $\chi^2$ , a distribution with  $h$  degrees of freedom. Both SPI3 and SPI6 are autocorrelated as the Box–Pierce test was significant ( $p < 0.0001$ ) (Table 4). The main step in the ARIMA model is the identification of the different combinations of parameters, such as autoregressive terms ( $p$ ), differencing terms ( $d$ ), and moving average terms ( $q$ ). A combination of the order of the parameters which has maximum log-likelihood and lowest values of Akaike information criteria (AIC) and Bayesian information criteria (BIC) is considered the best model. Along with log-likelihood, AIC and BIC criteria’s ACF

and PACF plots were also used (Figures S1–S4) for model order identification. The results are presented in Table 4. For SPI3 and SPI6 the best fitted ARIMA model was (1,0,2) and (1,0,0) with maximum log-likelihood of  $-544.14$  and  $-479.53$ , minimum AIC and BIC values are 1096.27 and 1112.79 for SPI3 and 963.07 and 971.31 for SPI6. After ARIMA model fitting, the diagnostic checking of residuals was carried out using the Box–Pierce non-correlation test, and residuals under consideration are non-correlated in nature as the probability of significance are  $p = 0.938$  and  $p = 0.779$  for SPI3 and SPI6, respectively.

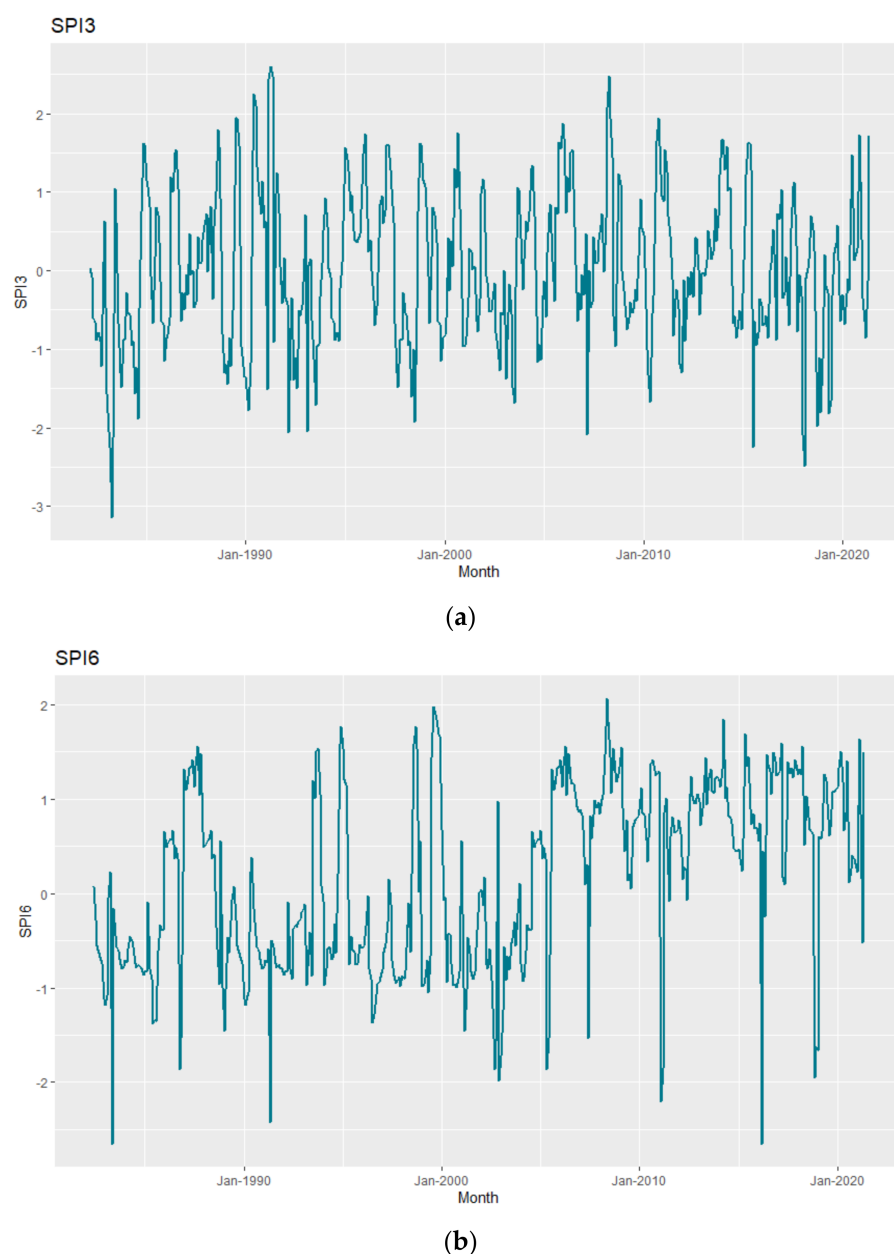


**Figure 4.** (a) Time series plot for SPI3; (b) time series plot for SPI6.

For building the AI model, the nonlinearity of the original data set was tested using the BDS test [42]. The results of the BDS test are shown in Table 5 and confirm that the data under consideration is nonlinear in nature as the probability of significance of residuals is  $p < 0.0001$ .

**Table 4.** Parameter estimation of ARIMA by maximum likelihood method for SPI3 and SPI6 time scales of Hyderabad region.

Time Scales	Model	Parameters	Estimation	S. E	Z Value	Prob.	Model Fitting	Box–Pierce Non-Correlation Test
SPI3	ARIMA (1,0,2)	AR1	−0.018	0.130	−0.143	$p < 0.0001$	Log likelihood −544.14	Original Residuals
		MA1	0.674	0.121	5.559	$p < 0.0001$	BIC 1112.79	Chi-square = 148.39 ( $p < 0.001$ )
		MA2	0.393	0.066	5.956	$p < 0.0001$	AIC 1096.27	Chi-square = 0.005 ( $p = 0.938$ )
SPI6	ARIMA (1,0,0)	AR1	0.717	0.032	22.03	$p < 0.0001$	Log likelihood −479.53	Chi-square = 233.19 ( $p < 0.001$ )
							AIC 963.07	Chi-square = 0.078 ( $p = 0.779$ )
							BIC 971.31	

SPI: standardized precipitation index, ARIMA: auto-regressive integrated moving average, AR: autoregressive, MA: moving average, S.E: standard error, prob. ( $p$ ): probability, BIC: Bayesian information criterion, AIC: Akaike information criterion.

**Table 5.** BDS test for non-linearity.

Sample	Dimension	SPI3		SPI6	
		Statistics	Probability	Statistics	Probability
eps(1)	$m = 2$	15.63	$p < 0.0001$	15.68	$p < 0.0001$
	$m = 3$	15.37	$p < 0.0001$	18.09	$p < 0.0001$
eps(2)	$m = 2$	14.23	$p < 0.0001$	12.72	$p < 0.0001$
	$m = 3$	13.11	$p < 0.0001$	12.09	$p < 0.0001$
eps(3)	$m = 2$	13.90	$p < 0.0001$	12.51	$p < 0.0001$
	$m = 3$	12.34	$p < 0.0001$	11.18	$p < 0.0001$
eps(4)	$m = 2$	15.40	$p < 0.0001$	13.92	$p < 0.0001$
	$m = 3$	13.76	$p < 0.0001$	12.43	$p < 0.0001$

eps: epsilon values (standard deviation of input variable as sample),  $m$ : embedded dimension,  $p$ : probability.

### 3.3. ANN Model

ANN model parameters are given in Table 6 for both SPI3 and SPI6 time scales. The drought indices of time series were subjected to ANN model with 5 and 4 tapped time delays and 2 and 4 optimum nodes for SPI3 and SPI6, respectively. Sigmoidal activation function in input to the hidden layer and linear identity function in hidden layers to output layer was used with feed-forward network architecture. The total number of parameters or weights obtained was 15 and 25 for SPI3 and SPI6, respectively. Diagnosis checking of residuals by Box–Pierce non-correlation test, which indicates the non-auto correlated or random nature of the residuals ( $p = 0.83$  and  $p = 0.72$ ) for SPI3 and SPI6 was done.

**Table 6.** Parameter specification of ANN model.

Parameters	SPI3	SPI6
Input lag	5	4
Output variable/dependent	1	1
Hidden nodes	1	1
Hidden layers	2	4
Model	(5:2S:1L)	(4:4S:1L)
Total number of parameters	15	25
Network type	Feed forward	Feed forward
Activation function (I:H)	Sigmoidal	Sigmoidal
Activation function (H:O)	Identity	Identity
Box–pierce non-correlation test for residuals	0.018	0.124
$p$ -value	0.873	0.724

I: input node, H: hidden node, S: sigmoidal activation function used in input to the hidden layer, L: linear unit activation function used in hidden to the output layer,  $p$ -value: probability value.

### 3.4. SVR Model

For the SVR model, parameters were considered based on the least RMSE values. The parameter specifications are listed in Table 7 for both SPI3 and SPI6 timescales, where the radial basis function (RBF) was used as a kernel function, and the number of support vectors obtained are 451 and 337, respectively. The cost function, gamma, and epsilon are 7.9, 0.16, and 0.01 for SPI3, and 7.7, 0.16, and 0.1 for SPI6, respectively. Box–Pierce tests done for diagnostic checking of residuals are random and white noise in nature as  $p = 0.27$  and 0.53 for both SPI3 and SPI6, respectively.

**Table 7.** Parameter specification of SVM model.

Model	SPI3	SPI6
Parameters	Values	Values
Kernel function	RBF	RBF
No. of S. V's	451	337
Cost	7.9	7.7
Gamma	0.16	0.16
Epsilon	0.01	0.1
Cross validation error	0.043	0.029
Box–Pierce non-correlation test for residuals	0.19	0.31
$p$ -value	0.27	0.57

RBF: radial basis function,  $p$ -value: probability value.

## 4. Discussion

Drought characterization by using SPI3 and SPI6 timescales indicated different categories of water stresses, i.e., moderately dry, severely dry, and extremely dry. Ten months showed extreme water stress in SPI3 and four months showed water stress on the SPI6 time scale, which indicates high water scarcity during the reported period (Table 8). Similar results for different classes of droughts and different time scales were also reported in [43–50].

**Table 8.** Classification of drought categories in SPI3 and SPI6.

Category	SPI3	SPI6
Extremely wet	-	-
Very wet	-	-
Moderately wet	-	-
Near normal	-	-
Moderately dry	Oct-1982, Sep-1983, Oct-1983, Jul-1984, Dec-1985, Dec-1988, Jan-1989, Feb-1989, Apr-1989, Nov-1989, Dec-1989, Jan-1990, Apr-1990, Jun-1992, Jul-1992, Jun-1993, Oct-1994, Aug-1997, Sep-1997, Jun-1998, Nov-1999, Oct-2002, Mar-2003, Jun-2003, Sep-2004, Nov-2004, Apr-2010, Sep-2018, Nov-2018, Jan-2019	Jan-1983, Feb-1983, Jun-1985, Jul-1985, Aug-1985, Jan-1989, Feb-1989, Mar-1989, Jan-1990, Feb-1990, Jul-1996, Aug-1996, Sep-1996, Feb-2000, Nov-2000, Dec-2000, Aug-2002, Feb-2003
Severely dry	Jan-1983, Jun-1984, Aug-1984, Feb-1990, Mar-1990, Mar-1991, May-1998, Jul-1998, Jul-2003, May-2010, Oct-2018, Dec-2018, May-2019, Jun-2019	Oct-1986, Nov-1986, Sep-2002, Oct-2002, Dec-2002, Jan-2003, Jun-2007, Mar-2011, Nov-2018, Dec-2018, Jan-2019
Extremely dry	Feb-1983, Mar-1983, May-1983, Mar-1992, Mar-1993, Jul-1993, Mar-2007, Jul-2015, Jan-2018, Feb-2018	May-1983, May-1991, Feb-2011, Mar-2016

The modelling and forecasting of SPI3 and SPI6 were compared in terms of MSE, RMSE for both training and testing sets for SPI3 and SPI6, respectively. AI models outperformed the classical model, SVR model was found to be superior over ARIMA and ANN models in training and testing sets for both SPEI3 and SPEI6. Performance hierarchy of these models is as follows: SVR > ANN > ARIMA in both training and validation sets. The detailed comparison of modelling and forecasting performance of different models in training and testing sets are depicted in Tables 9 and 10. Forecasted values and model comparison criteria of testing data sets are given in Table 10. Further, actual vs. fitted data of both training and testing sets are given in Table S2 and are also plotted in Figure 5a,b for drought in both SPI3 and SPI6 time scales, respectively. Similar results were obtained in [51–54], where the SVR model outperformed ARIMA and ANN models.

**Table 9.** Model comparison for training data for SPI3 and SPI6.

Model	Parameter	ARIMA	ANN	SVR
SPI3	MSE	0.438	0.418	0.378
	RMSE	0.496	0.459	0.413
SPI6	MSE	0.328	0.275	0.237
	RMSE	0.363	0.317	0.289

MSE: mean square error, RMSE: root mean square error.

**Table 10.** Model comparison for testing data for SPI3 and SPI6.

Period	Actual		Forecasted					
			ARIMA		ANN		SVR	
	SPI3	SPI6	SPI3	SPI6	SPI3	SPI6	SPI3	SPI6
Jun-20	0.917	0.851	0.241	0.083	0.132	0.254	0.197	0.064
Jul-20	1.477	1.418	0.194	0.11	0.07	0.182	0.713	0.669
Aug-20	0.133	0.12	−0.004	0.082	−0.089	0.131	0.554	0.83
Sep-20	0.226	0.262	−0.689	0.085	−0.068	0.094	−0.085	0.352
Oct-20	0.279	0.400	−0.812	0.059	−0.083	0.067	−0.186	−0.501
Nov-20	1.734	0.369	−0.987	0.433	0.357	0.048	0.403	0.338
Dec-20	1.142	0.322	−0.988	0.025	−0.072	0.035	0.87	0.294
Jan-21	−0.342	0.23	−0.567	0.096	−0.069	0.025	−0.549	0.25
Feb-21	−0.636	1.646	−0.288	−0.028	−0.074	0.018	−0.804	0.839
Mar-21	−0.853	0.84	−0.755	−0.013	−0.07	0.013	−0.025	1.416
Apr-21	−0.138	−0.526	1.988	−0.02	−0.072	0.009	−0.994	0.399
May-21	1.709	1.491	1.832	−0.025	−0.07	0.007	−0.111	0.227
			MSE					
			1.317	0.72	0.867	0.672	0.686	0.495
			RMSE					
			1.734	0.848	0.931	0.82	0.828	0.703

MSE: mean square error, RMSE: root mean square error.

The ANN for water stress modeling was developed with the ‘Levenberg–Marquardt backpropagation algorithm’ in a feed-forward network based on repetitive iterations. The user-defined hyper-parameters for ANN model, such as learning rate and momentum, were fixed based on repetitive experimentation as 0.04 and 0.001, respectively. To obtain the stable model, the network was repeated 30 times with 1250 iterations. The candidate input lags and hidden nodes were determined based on the lowest training errors. Tenfold cross-validation was carried out for each model and the lowest cross-validation error obtained is reported in Tables 6 and 7. For SPI3 and SPI6 time scales we tuned the model with different permutations and combinations of hyper-parameters and chose the candidate parameters based on the lowest training MSE and RMSE. A similar procedure was followed in [55] for building ANN and SVR models.

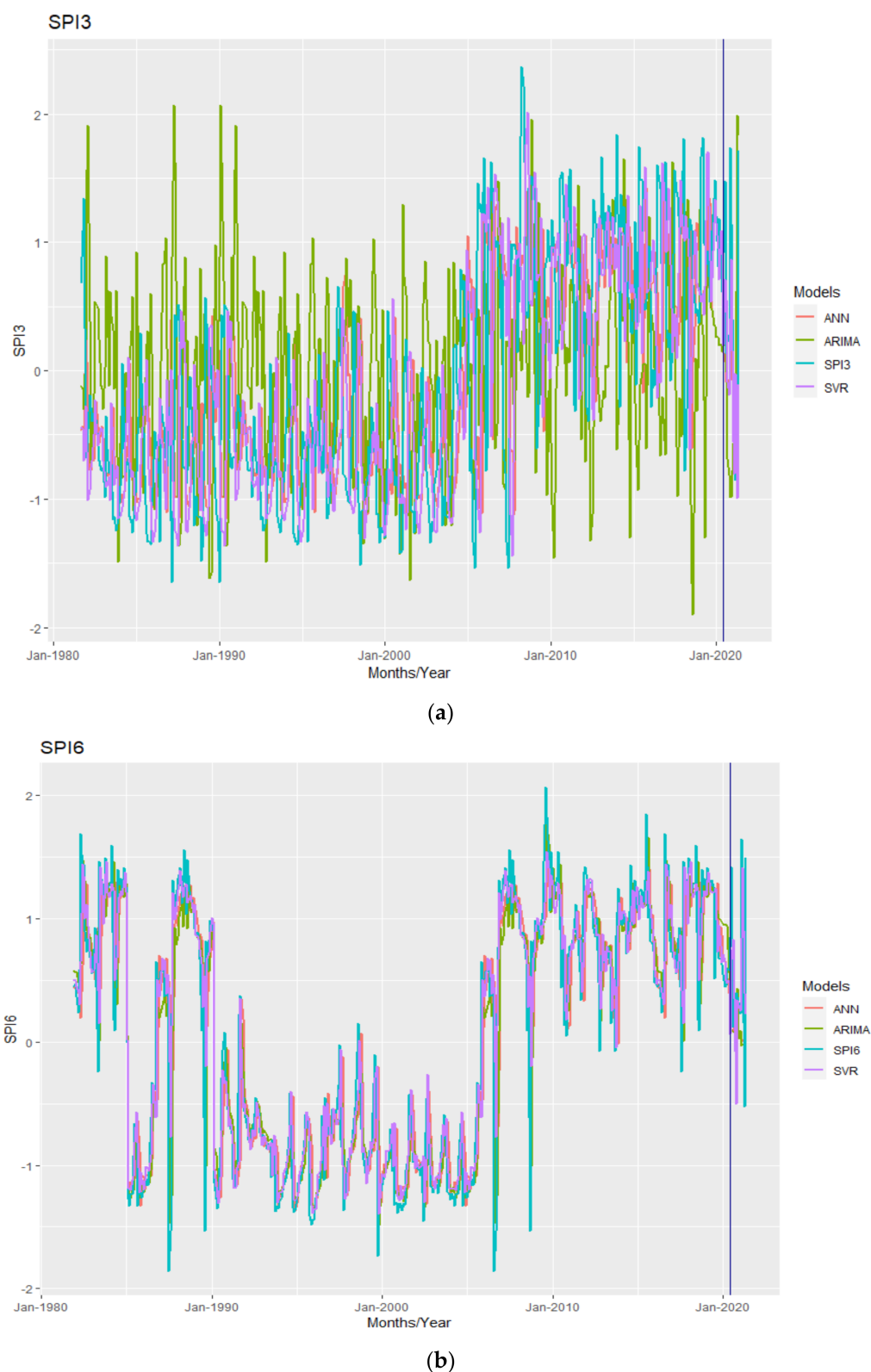


**Figure 5.** (a) Actual vs. fitted plots of SPI3; (b) actual vs. fitted plots of SPI6.

The comparison criteria, viz., MSE and RMSE exhibit only the observed differences between the predicted values of the models. The DM test statistics were used to determine the statistically significant differences among the models used. The ARIMA (M1) and ANN (M2) models are significantly different with respect to SVR (M3) model for both SPI3 and SPI6. Inter combinational significances are clearly mentioned in Table 11 for both SPI3 and

SPI6. The performance of SVR model is significantly superior to the other two models in the input and testing data sets for both SPI3 and SPI6. These results may be due to the ability of the SVR model to account for the nonlinear and complex patterns in the input data sets, which can be a comprehensive tool for managing and alleviating water stress in plants. Similarly, the DM test was applied in [27,56,57] for significant comparison of modeling performance of the developed model in both training and validation data sets.

**Table 11.** Diebold–Mariano (DM) test for comparing performance of different time series models for training and testing data set for both SPI3 and SPI6.

Model	Data Type	M1, M2	M1, M3	M2, M3
SPI3	Training set	5.62 ( $p < 0.0001$ )	5.05 ( $p < 0.0001$ )	−0.38 ( $p < 0.0001$ )
	Testing set	3.67 ( $p < 0.0001$ )	2.57 ( $p < 0.0001$ )	−0.12 ( $p < 0.0001$ )
SPI6	Training set	7.77 ( $p < 0.0001$ )	6.24 ( $p < 0.0001$ )	4.07 ( $p < 0.0001$ )
	Testing set	0.75 ( $p < 0.0001$ )	0.62 ( $p < 0.0001$ )	0.52 ( $p < 0.0001$ )

M1: ARIMA, M2: ANN, M3: SVR,  $p$ : probability value.

## 5. Conclusions

The present study was carried out to understand the short and medium-term water stress in agroecosystems of the Hyderabad region using SPI3 and SPI6 timescales. The results showed that during the period 1982–2021, 13 months were identified as severe drought, 10 months as extreme drought, and 29 months as moderate drought on the short-term scale (SPI3). Similarly, the medium-term drought index (SPI6) identified 4 months as extreme drought, 11 months as severe drought, and 18 months as moderate water stress during the period 1982–2021. In addition, classical models and AI models were used to predict water stress, confirming that among the AI models, SVR performs better vs. ANN, and the classical ARIMA model in terms of MSE and RMSE. The results can be a very useful tool for management and planning at the regional/national level of water (stress) as one of the most important and critical resources in cropping systems. Due to the lack of availability of continuous historical data on other weather parameters for the study region, only rainfall data was used for estimating the drought index in this study. However, future studies need to be expanded with either weather (e.g., air temperature, solar radiation), hydrologic (e.g., water table), agronomic (e.g., yield reduction), or in combination, parameters to allow detailed characterization of drought using various machine learning-based models.

**Supplementary Materials:** The following supporting information can be downloaded at: <https://www.mdpi.com/article/10.3390/su14116690/s1>, Figure S1. Autocorrelation Function (ACF) plot of SPI3; Figure S2. Partial Autocorrelation Function (PACF) plot of SPI3; Figure S3. Autocorrelation Function (ACF) plot of SPI36; Figure S4. Partial Autocorrelation Function (PACF) plot of SPI6; Table S1. Calculated SPI3 and SPI6; Table S2. Actual vs. Fitted SPI.

**Author Contributions:** Data curation, A.G. and S.R.; formal analysis, A.G., R.P. and S.R.; investigation, A.G., S.K. and S.R.; methodology, A.G., S.K., P.D.S., R.P., N.B., G.O., M.A., C.G., M.S.A., B.P., B.K.Y., R.M.S. and S.R.; resources, S.K., R.M.S. and S.R.; software, A.G. and S.R.; supervision, S.K. and S.R.; visualization, G.O. and S.R.; writing—original draft, A.G.; writing—review and editing, S.K., P.D.S., R.P., N.B., G.O., M.A., C.G., M.S.A., B.P., B.K.Y., R.M.S. and S.R. All authors have read and agreed to the published version of the manuscript.

**Funding:** This research received no external funding.

**Institutional Review Board Statement:** Article approved for submission. Ref. No. IIRR/DIR/PD/PMEC/2021-22/Res.Paper/442 dt.15.02.2022.

**Informed Consent Statement:** Not applicable.

**Data Availability Statement:** The data presented in this study were collected from the reports of the Directorate of Economics and Statistics, Government of Telangana. The data presented in this study are available on request from the corresponding author.

**Acknowledgments:** The authors would like to thank ICAR (Indian Institute of Rice Research) Hyderabad and PJTSAU Hyderabad for their support in this research work.

**Conflicts of Interest:** The authors declare no conflict of interest.

## References

- Markulj Kulundžić, A.; ViljevacVuletić, M.; MatošaKočar, M.; Mijić, A.; Varga, I.; Sudarić, A.; Cesar, V.; Lepeduš, H. The Combination of Increased Temperatures and High Irradiation Causes Changes in Photosynthetic Efficiency. *Plants* **2021**, *10*, 2076. [CrossRef] [PubMed]
- Heim, R.R., Jr. A comparison of the early twenty-first century drought in the United States to the 1930s and 1950s drought episodes. *Bull. Am. Meteorol. Soc.* **2017**, *98*, 2579–2592. [CrossRef]
- Seleiman, M.F.; Al-Suhaibani, N.; Ali, N.; Akmal, M.; Alotaibi, M.; Refay, Y.; Dindaroglu, T.; Abdul-Wajid, H.H.; Battaglia, M.L. Drought Stress Impacts on Plants and Different Approaches to Alleviate Its Adverse Effects. *Plants* **2021**, *10*, 259. [CrossRef] [PubMed]
- Raza, A.; Razzaq, A.; Mehmood, S.S.; Zou, X.; Zhang, X.; Lv, Y.; Xu, J. Impact of Climate Change on Crops Adaptation and Strategies to Tackle Its Outcome: A Review. *Plants* **2019**, *8*, 34. [CrossRef] [PubMed]
- Raihan, F.; Ondrasek, G.; Islam, M.S.; Maina, J.M.; Beaumont, L.J. Combined Impacts of Climate and Land Use Changes on Long-Term Streamflow in the Upper Halda Basin, Bangladesh. *Sustainability* **2021**, *13*, 12067. [CrossRef]
- Ondrasek, G.; Rathod, S.; Manohara, K.K.; Gireesh, C.; Anantha, M.S.; Sakhare, A.S.; Parmar, B.; Yadav, B.K.; Bandumula, N.; Raihan, F.; et al. Salt Stress in Plants and Mitigation Approaches. *Plants* **2022**, *11*, 717. [CrossRef]
- Ondrasek, G. Water Scarcity and Water Stress in Agriculture. In *Physiological Mechanisms and Adaptation Strategies in Plants under Changing Environment*; Ahmad, P., Wani, M., Eds.; Springer: New York, NY, USA, 2014. [CrossRef]
- The State of Food and Agriculture: Climate Change, Agriculture and Food Security. Available online: <https://www.fao.org/3/i6030e/i6030e.pdf> (accessed on 4 March 2022).
- Mishra, A.K.; Singh, V.P. Drought Modeling—A Review. *J. Hydrol.* **2011**, *403*, 157–175. [CrossRef]
- McKee, T.B.; Doesken, N.J.; Kleist, J. The relationship of drought frequency and duration to time scales. In Proceedings of the 8th Conference on Applied Climatology, Anaheim, CA, USA, 17–22 January 1993; American Meteorological Society: Boston, MA, USA, 1993; Volume 17, pp. 179–183.
- Thom, H.C.S. *Some Methods of Climatological Analysis*; Secretariat of the World Meteorological Organization: Geneva, Switzerland, 1966.
- Jaber, A. Drought Analysis for Kuwait Using Standardized Precipitation Index. *Sci. World J.* **2014**, *2014*, 1–9. [CrossRef]
- Musonda, B.; Jing, Y.; Iyakaremye, V.; Ojara, M. Analysis of Long-Term Variations of Drought Characteristics Using Standardized Precipitation Index over Zambia. *Atmosphere* **2020**, *11*, 1268. [CrossRef]
- Jobin, T.; Prasannakumar, V. Temporal analysis of rainfall (1871–2012) and drought characteristics over a tropical monsoon-dominated State (Kerala) of India. *J. Hydrol.* **2016**, *534*, 266–280. [CrossRef]
- Caloiero, T.; Caroletti, G.N.; Coscarelli, R. IMERG-Based Meteorological Drought Analysis over Italy. *Climate* **2021**, *9*, 65. [CrossRef]
- Tien Thanh, N. A Proposal to Evaluate Drought Characteristics Using Multiple Climate Models for Multiple Timescales. *Climate* **2018**, *6*, 79. [CrossRef]
- Zhao, Q.; Chen, Q.; Jiao, M.; Wu, P.; Gao, X.; Ma, M.; Hong, Y. The Temporal-Spatial Characteristics of Drought in the Loess Plateau Using the Remote-Sensed TRMM Precipitation Data from 1998 to 2014. *Remote Sens.* **2018**, *10*, 838. [CrossRef]
- Pandey, V.; Srivastava, P.K.; Singh, S.K.; Petropoulos, G.P.; Mall, R.K. Drought Identification and Trend Analysis Using Long-Term CHIRPS Satellite Precipitation Product in Bundelkhand, India. *Sustainability* **2021**, *13*, 1042. [CrossRef]
- Guo, H.; Bao, A.; Liu, T.; Ndayisaba, F.; He, D.; Kurban, A.; Maeyer, P.D. Meteorological drought analysis in the Lower Mekong Basin using satellite based Long term CHIRPS product. *Sustainability* **2017**, *9*, 901. [CrossRef]
- Roman, R.; Ali, Y.; Joanna, K.; Atilgan, A.; Monika, M.; Daniel, L. Analysis of SPI as a drought indicator during the maize growing period in the cukurova region (Turkey). *Sustainability* **2022**, *14*, 3697. [CrossRef]
- Li, K.; Wang, M.; Liu, K. The study on compound heatwave events in china using complex networks. *Sustainability* **2021**, *13*, 12774. [CrossRef]
- Box, G.; Jenkins, G. *Time Series Analysis: Forecasting and Control*; Holden-Day: San Francisco, CA, USA, 1970.
- Morid, S.; Smakhtin, V.; Bagherzadeh, K. Drought forecasting using artificial neural networks and time series of drought indices. *Int. J. Climatol.* **2007**, *27*, 2103–2111. [CrossRef]
- Patil, R.; Polisgowdar, B.S.; Rathod, S.; Satish, K.U.; Srinivasa Reddy, G.V.; Vijaya, W.; Satyanarayana, R. Drought Modelling and Forecasting using Arima and Neural Networks for Ballari District, Karnataka. *J. Indian Soc. Agric. Stat.* **2020**, *74*, 149–157.
- Rathod, S.; Singh, K.N.; Arya, P.; Ray, M.; Mukherjee, A.; Sinha, K.; Kumar, P.; Shekhawat, R.S. Forecasting maize yield using ARIMA-Genetic Algorithm approach. *J. Outlook Agr.* **2017**, *46*, 265–271. [CrossRef]
- Rathod, S.; Mishra, G.C. Statistical Models for Forecasting Mango and Banana Yield of Karnataka, India. *J. Agric. Sci. Technol.* **2018**, *20*, 803–816.

27. Patil, R.; Nagaraj, D.M.; Polisgowdar, B.S.; Rathod, S. Forecasting potential evapotranspiration for Raichur district using seasonal ARIMA model. *Mausam* **2022**, *73*, 433–440. [CrossRef]
28. Rathod, S.; Saha, A.; Patil, R.; Ondrasek, G.; Gireesh, C.; Anantha, M.S.; Rao, D.V.K.N.; Nirmala, B.; Senguttuvel, P.; Arun, K.S.; et al. Two-Stage Spatiotemporal Time Series Modelling Approach for Rice Yield Prediction & Advanced Agroecosystem Management. *Agronomy* **2021**, *11*, 2502. [CrossRef]
29. Naveena, K.; Singh, S.; Rathod, S.; Singh, A. Hybrid ARIMA-ANN Modelling for forecasting the price of Robusta Coffee in India. *Int. J. Curr. Microbiol. App. Sci.* **2017**, *6*, 1721–1726. [CrossRef]
30. Saha, A.; Singh, K.N.; Ray, M.; Rathod, S. A hybrid spatio-temporal modelling: An application to space-time rainfall forecasting. *Theor. App. Climat.* **2020**, *142*, 1271–1282. [CrossRef]
31. Zhu, Q.; Luo, Y.; Zhou, D.; Xu, Y.; Wang, G.; Tian, Y. Drought prediction using in situ and remote sensing products with SVM over the Xiang River Basin, China. *Nat. Hazards* **2020**, *105*, 2161–2185. [CrossRef]
32. Alam, W.; Ray, M.; Kumar, R.R.; Sinha, K.S.; Rathod, S.; Singh, K.N. Improved ARIMAX modal based on ANN and SVM approaches for forecasting rice yield using weather variables. *Indian J. Agric. Sci.* **2018**, *88*, 1909–1913.
33. Alam, W.; Sinha, K.; Kumar, R.R.; Ray, M.; Rathod, S.; Singh, K.N.; Arya, P. Hybrid linear time series approach for long term forecasting of crop yield. *Indian J. Agric. Sci.* **2018**, *88*, 1275–1279.
34. Zhang, Y.; Yang, H.; Cui, H.; Chen, Q. Comparison of the Ability of ARIMA, WNN and SVM Models for Drought Forecasting in the Sanjiang Plain, China. *Nat. Reso. Rese.* **2019**, *29*, 1447–1464. [CrossRef]
35. Saha, A.; Singh, K.N.; Ray, M.; Rathod, S.; Choudhury, S. Modelling and forecasting cotton production using tuned-support vector regression. *Curr. Sci.* **2021**, *121*, 1090. [CrossRef]
36. Chakraborty, S.; Goyal, M.; Rao, A.; Sen, S.; Jain, S.; Manoj, J. *Drought Preparedness of Vulnerable Sections in Rural Telangana*; South Asia Consortium for Interdisciplinary Water Resources Studies: Secunderabad, India, 2018; Available online: <http://www.saciwaters.org/pdfs/DPVSRT.pdf> (accessed on 6 March 2022).
37. Diebold, F.X.; Mariano, R.S. Comparing predictive accuracy. *J. Bus. Econ. Stat.* **1995**, *13*, 253–263.
38. Abramowitz, M.; Stegun, I.A. *Handbook of Mathematical Functions with Formulas, Graphs and Mathematical Table*; Courier Dover Publications: New York, NY, USA, 1965.
39. Zhang, G.P. Time series forecasting using a hybrid ARIMA and neural network model. *Neurocomputing* **2003**, *50*, 159–175. [CrossRef]
40. Zhang, G.; Eddy Patuwo, B.; Hu, Y.M. Forecasting with artificial neural networks: The state of the art. *Int. J. Forecast.* **1998**, *14*, 35–62. [CrossRef]
41. Rathod, S.; Singh, K.N.; Patil, S.G.; Naik, R.H.; Ray, M.; Meena, V.S. Modelling and forecasting of oilseed production of India through artificial intelligence techniques. *Indian J. Agric. Sci.* **2018**, *88*, 22–27.
42. Vapnik, V.N. *The Nature of Statistical Learning Theory*; Springer: New York, NY, USA, 1995.
43. Brock, W.; Scheinkman, J.A.; Dechert, W.D.; LeBaron, B. A Test for Independence Based on the Correlation Dimension. *Eco. Rev.* **1996**, *15*, 197–235. [CrossRef]
44. Leszek, L. Estimation of local drought frequency in central Poland using the standardized precipitation index SPI. *Irrig. Drain.* **2007**, *56*, 67–77. [CrossRef]
45. Thomas, T.; Jaiswal, R.K.; Nayak, P.C.; Ghosh, N.C. Comprehensive evaluation of the changing drought characteristics in Bundelkhand region of Central India. *Meteor. Atmos. Phys.* **2015**, *127*, 163–182. [CrossRef]
46. Botai, C.; Botai, J.; de Wit, J.; Ncongwane, K.; Adeola, A. Drought Characteristics over the Western Cape Province, South Africa. *Water* **2017**, *9*, 876. [CrossRef]
47. Caloiero, T.; Veltri, S.; Caloiero, P.; Frustaci, F. Drought Analysis in Europe and in the Mediterranean Basin Using the Standardized Precipitation Index. *Water* **2018**, *10*, 1043. [CrossRef]
48. Xia, L.; Zhao, F.; Mao, K.; Yuan, Z.; Zuo, Z.; Xu, T. SPI-Based Analyses of Drought Changes over the Past 60 Years in China's Major Crop-Growing Areas. *Remote Sens.* **2018**, *10*, 171. [CrossRef]
49. Sobral, B.S.; de Oliveira-Junior, J.S.; de Gois, G.; Pereira-Junior, E.R.; de BodasTerassi, P.M.; Muniz-Junior, J.G.R.; Lyra, G.B.; Zeri, M. Drought characterization for the state of Rio de Janeiro based on the annual SPI index: Trends, statistical tests and its relation with ENSO. *Atmos. Res.* **2019**, *220*, 141–154. [CrossRef]
50. Pei, Z.; Fang, S.; Wang, L.; Yang, W. Comparative Analysis of Drought Indicated by the SPI and SPEI at Various Timescales in Inner Mongolia, China. *Water* **2020**, *12*, 1925. [CrossRef]
51. Falak, N.; Dars, G.H.; Ansari, K.; Jamro, S.; Nir, Y.K. Drought trends in Balochistan. *Water* **2020**, *12*, 470. [CrossRef]
52. Borji, M.; Malekian, A.; Salajegheh, A.; Ghadimi, M. Multi-time-scale analysis of hydrological drought forecasting using support vector regression (SVR) and artificial neural networks (ANN). *Arab. J. Geosci.* **2016**, *9*, 725. [CrossRef]
53. Mokhtarzad, M.; Eskandari, F.; Jamshidi, V.N.; Arabasadi, A. Drought forecasting by ANN, ANFIS, and SVM and comparison of the models. *Environ. Earth Sci.* **2017**, *76*, 729. [CrossRef]
54. Rathod, S.; Mishra, G.; Singh, K.N. Hybrid time series models for forecasting banana production in Karnataka state, India. *J. Indian Soc. Agric. Stat.* **2017**, *71*, 193–200.
55. Khan, N.; Sachindra, D.A.; Shahid, S.; Ahmed, K.; Shiru, M.S.; Nawaz, N. Prediction of droughts over Pakistan using machine learning algorithms. *Adva. Water Reso.* **2020**, *139*, 103562. [CrossRef]

- 
56. Rathod, S.; Yerram, S.; Arya, P.; Katti, G.; Rani, J.; Padmakumari, A.P.; Somasekhar, N.; Padmavathi, C.; Ondrasek, G.; Amdan, S.; et al. Climate-Based Modeling and Prediction of Rice Gall Midge Populations Using Count Time Series and Machine Learning approaches. *Agronomy* **2022**, *12*, 22. [[CrossRef](#)]
  57. Chitikela, G.; Meena, A.; Vijaya, K.R.; Nirmala, B.; Gabrijel, O.; Raman, M.S.; Rathod, S. Artificial-Intelligence-Based Time-Series Intervention Models to Assess the Impact of the COVID-19 Pandemic on Tomato Supply and Prices in Hyderabad, India. *Agronomy* **2020**, *11*, 1878. [[CrossRef](#)]